Plasmonic Structures Fabricated by Interference Lithography for Sensor Applications

Jacson W. Menezes*[a,b], Marcelo Nalin[c], Enver F. Chillcce[b], Edmundo S. Braga[a] and Lucila Cescato[b]
[a]School of Electrical and Computer Engineering, Unicamp, Campinas-SP Brazil 13081-970
[b]Institute of Physics Gleb Wataghin, Unicamp, Campinas-SP Brazil 13083-970
[c]Department of Physics, UNESP, Bauru-SP, Brazil 17033-360

ABSTRACT

In this work we demonstrate the use of holographic lithography for generation of large area plasmonic periodic structures. Submicrometric array of holes, with different periods and thickness, were recorded in gold films, in areas of about 1 cm^2, with homogeneity similar to that of samples recorded by Focused Ion Beam. In order to check the plasmonic properties, we measured the transmission spectra of the samples. The spectra exhibit the typical surface plasmon resonances (SPR) in the infrared whose position and width present the expected behavior with the period of the array and film thickness. The shift of the peak position with the permittivity of the surrounding medium demonstrates the feasebility of the sample as large area sensors.

Keywords: Holography, Microfabrication, Plasmonic structures, surface plasmon resonance

1- INTRODUCTION

Surface plasmons (SP) are surface bound electromagnetic waves that can be excited in metallic nanostructures using visible radiation [1-4]. The ability to pattern nanoscale metal structures presents an opportunity to tailor surface plasmon response to specific applications [3-6]. When the incident electromagnetic wave matches the conservation of momentum, a surface plasmon mode is excited. This surface plasmon produces an enhancement in the transmitted light that depends strongly of the relative permittivity of the metal and the surrounding medium [2]. In this way, periodic arrays of nanoholes in thin films of gold can be used as Surface Plasmons Resonance (SPR) sensors that operate in transmission mode [6].

Nanoholes in metal films have been fabricated mainly through focused ion beam (FIB) milling [1,2,5,6]. This technique allows one-step nanofabrication with precise control of the hole size and placement, and the fabrication of highly ordered arrays with well defined geometry. However, because of the serial nature of the FIB process, the maximum area of the fabricated samples is about 100 x 100μm. This is a serious constraint for sensor applications because it requires the use of focused light in order to concentrate the light in the sample as well as it requires the manipulation of the samples in small areas. These factors limit the commercial feasibility of the nanohole array structures produced using FIB. For generation of high-resolution periodic structures in large areas the holographic lithography appears as an interesting alternative.

The simplest way for generation two-dimensional patterns by holography is the double exposure of a photoresist film to the same interference pattern produced by the interference of two beams. The superimposition of interference patterns generated by two-beams [7,8] presents several advantages in relation to a single exposure of multiple beams: a) The setup is easier because it employs two co-planar beams instead of aerial multiple beams; b) The interfering beams can be taken with the same polarization (increasing the contrast of the interference pattern); c) It is possible to lock the interference pattern during the exposure by controlling the phase difference between the two beams. Such advantages result in higher contrast of the intensity light pattern allowing the recording of high aspect ratio structures. Besides this fact, homogeneous fringe patterns, with low distortion, can be obtained in large areas.

Plasmonics: Metallic Nanostructures and Their Optical Properties VII, edited by Mark I. Stockman,
Proc. of SPIE Vol. 7394, 73942M · © 2009 SPIE · CCC code: 0277-786X/09/$18 · doi: 10.1117/12.826129

In this work, we recorded large area plasmonic structures using the combination of a high contrast holographic lithography, to generate a high aspect ratio photoresist template, followed by the evaporation of thin Au film and the "lift-off" process of the photoresist template.

2- THE INTERFERENCE LITHOGRAPHY

The interference lithography consists in to expose a photosensitive material to a fringe pattern, generated by the interference of two coherent beams. To generate a squared pattern the material is exposed twice to the same fringe pattern, with rotation of the sample of 90^0 between the exposures.

The light dose (E_R) inside a photosensitive material, resulting from the multiple exposures of interference patterns is the sum of the light intensity I_{Ri} of each interference pattern multiplied by the time of each exposure (Δt_i).

$$E_R = \sum_{i=1}^{n} (\Delta t_i) I_{Ri} \tag{1}$$

Assuming that the interference pattern is generated by two plane wave-fronts with equal irradiance $I_1=I_2=I$, forming an angle 2θ between them (Figure 1), neglecting the absorption of the photosensitive material and considering that the sample may rotate of an angle α_i around the "z" axis (bisector of the interfering beams – Figure 1), the resultant irradiance I_{Ri} of each interference pattern can be represented by:

$$I_R = 2I\left\{ n + \sum_{i=1}^{n} \cos\left[\frac{2\pi}{\Lambda_i} \left(\cos(\alpha_i)\, x - \sin(\alpha_i)\, y \right) + \phi_i \right] \right\} \tag{2}$$

with Λ_i being the fringe period of each exposure that is determined by the angle θ between the interfering beams (Figure 1), α_i is the rotation angle of the sample measured in relation to the x axis, for each exposure and ϕ_i the relative phase of each fringe pattern. When the sample is rotated of $\alpha=90^o$ between two exposures, square lattice may be recorded. In the case of two exposures, any phase shift ϕ introduced in the second fringe pattern only shifts the whole pattern, but do not change the shape of the light patterns. Figure 2 shows the simulated light patterns resulting from the superimposition of two sinusoidal fringe patterns rotated of $(\alpha_1,\alpha_2)=(0^o,90^o)$ between the exposures. Here, the simulated pattern have same period ($\Lambda_1=\Lambda_2=0.7\mu m$) and same time of exposure $\Delta t_1=\Delta t_2$. If we choose an intensity threshold I, we can get a certain lattice.

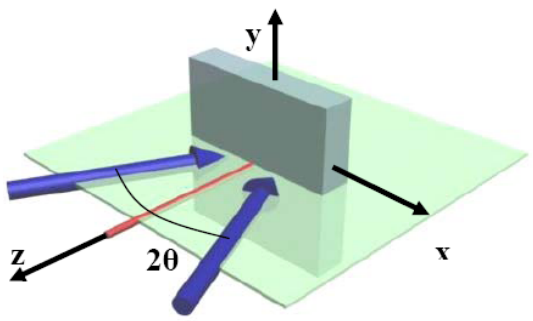

Fig. 1. Scheme of the interfering beams and sample positioning. Note that the rotation axis "z" of the sample is also the bisector of the interfering beams.

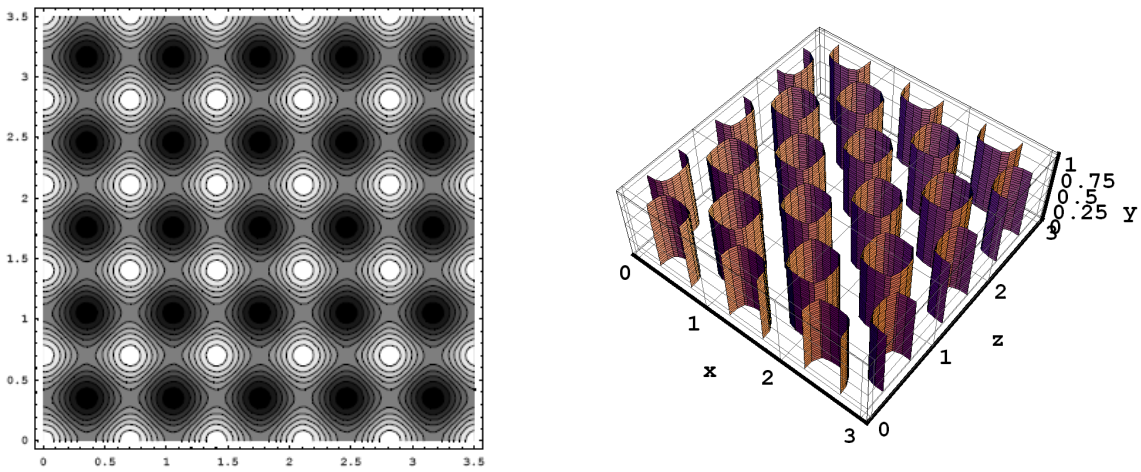

Fig. 2. Simulated light pattern resulting from the superimposition of two interference patterns using α_1=0 o and α_2=90^o. (a) iso-curves and (b) one-dose

The experimental procedure employed for recording of plasmonic structures is schematized in Figure 3. In the first step, the positive photoresist (SC 1827 Rohm and Haas) film was deposited by spin coating technique on a glass substrate, using a rotation of 3500 rpm for 30s, resulting in a film thickness of about 0.6 μm. The photoresist was then exposed twice, by rotating the sample of 90° between each exposure, using the superimposition of two interference patterns generated by a setup holographic (Figure 4) using the line λ = 458 nm of a 300 mW Melles Griot solid state laser. This setup allows the recording of any fringe period from 450 nm to 1800 nm and it is provided with a fringe locker system which warrants the repeatability and the high contrast of the fringes [9]. After the double exposure at the same dose of 350mJ/cm^2, the photoresist film was developed in AZ Developer diluted 1:4 during 40 seconds in order to obtain the photoresist template. The last step is the thermal evaporation of the thin Au film, followed by the lift-off process of the photoresist template.

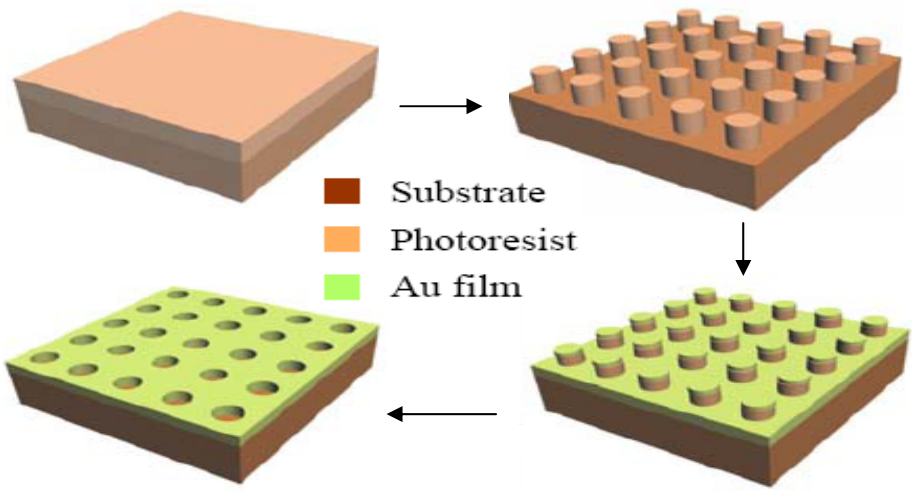

Fig. 3. Steps of the fabrication process.

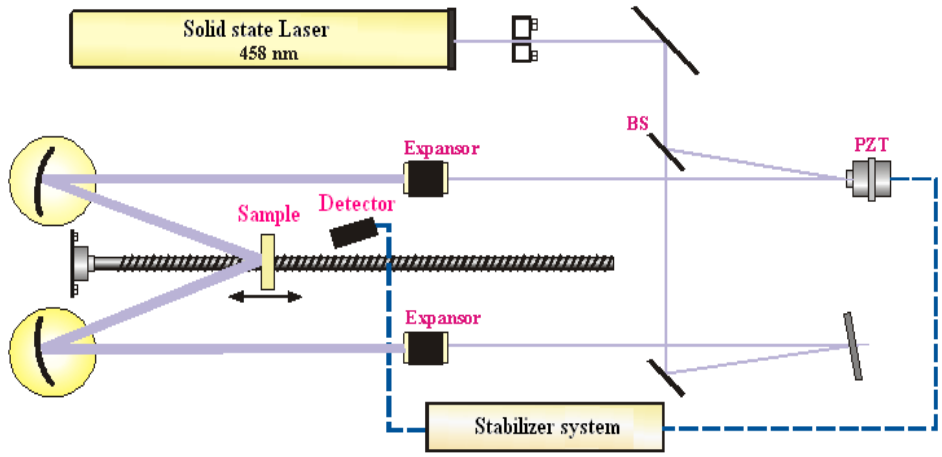

Fig. 4. Scheme of the holographic setup used to record the periodic structures.

Two samples with different periods were fabricated: The first sample with period of Λ=600nm and the second sample with period of Λ=700nm. The Scanning Electron Microscopy (SEM) photographs of the cross-section and top view of the structures recorded in photoresist with period of 600nm is shown in Figure 5(a). The photoresist template is constituted of well-defined columns, measuring around 0.6 μm of high. This is a necessary characteristic for the lift-off process. Controlling the process of thermal evaporation on the two samples (600nm and 700nm), two different thicknesses of the thin Au film were obtained for each sample: t~100nm and t~200nm. Figure 5(b) shows the SEM photograph of the resulting 2D squared lattice after the lift-off of photoresist template using acetone. The samples are homogeneous in an area of about 1 inch squared.

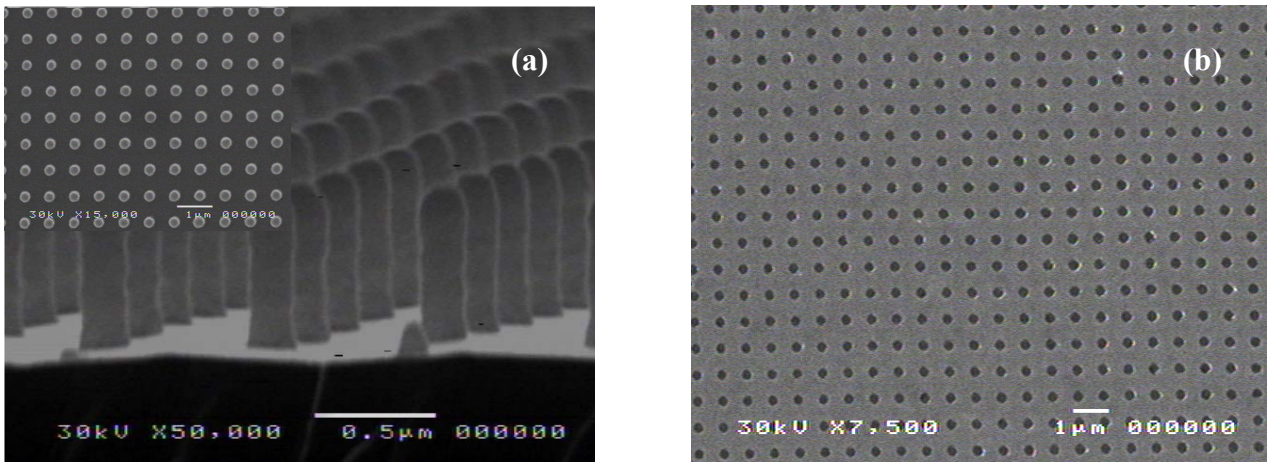

Fig. 5. SEM photograph of the (a) cross-section of the two-dimensional squared lattice photoresist templates on glass substrate. The inset shows the top view of the sample and (b) top view of the sample after lift-off process

The measurement of the hole-size distribution was realized using digitalized SEM photographs of random areas of the sample with periodicity of 700nm and the image analysis was done using the program Image Pro-Plus version 4.5 (Media Cybernetics, Inc.). The histogram results in a mean hole diameter (M) of 312 nm, and a standard deviation (σ) of 16 nm (figure 6). The holes present a coefficient of variation (CV = σ/M) of 5.12%. This CV represents an extremely low dispersion, comparable the structures recorded by e-beam or FIB.

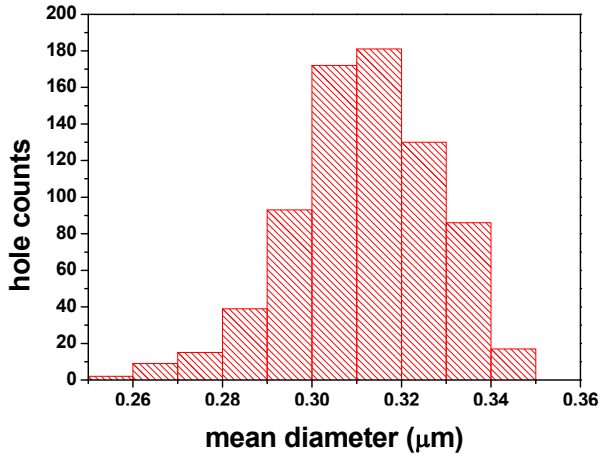

Fig. 6. Measurement of the hole-size distribution using digitalized SEM photographs of random areas of the sample with periodicity of 700nm

3- THE OPTICAL MEASUREMENTS

The transmission spectra of the squared arrays of holes were measured using an Optical Spectrum Analyzer (OSA) *YOKOGAWA* AQ-6315A. Figure 7 shows the transmission spectra of samples with periods of 600 nm and 700 nm and two different thickness of the Au film (t = 100nm and t = 200nm), for normal incidence. By comparing the spectra, we observed that for the same Au thickness, there is a shift of the plasmonic peak to the infrared for the larger period sample. This occurs because the wavelength position of the peak is directly proportional to the period of the array (Λ) [2]. The wavelength positions of the peaks are presented in Table I. As it can be observed from these values, for an increasing in the array period of 16 % (from 600 to 700 nm) there is an increasing in the peak wavelength of 18 % (for the 200nm film thickness) and 15 % (for the 100 nm film thickness). On the other hand, there is a narrowing of the peak when the film thickness increases while the amplitude decreases. The well definition of the plasmonic peaks indicates a good homogeneity of the sample in whole measured area (about 5mm^2).

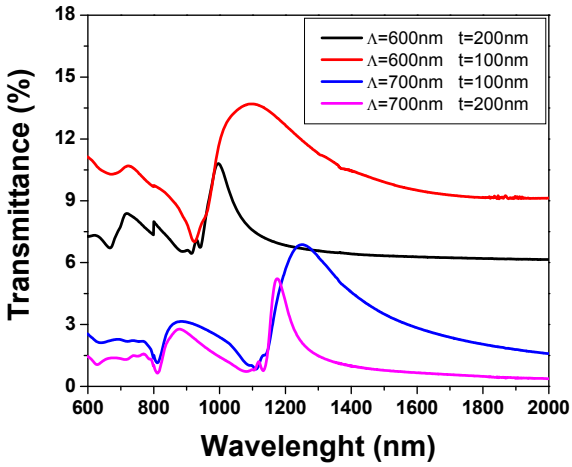

Fig. 7. Transmission spectra of the samples with different periods and thicknesses.

Figure 8 shows the transmission spectra for different angles of incidence in the plane that contain the grating vector G_x, for the samples with period Λ = 700 nm and two different Au film thickness: 100 nm and 200 nm, Figure 8 (a) and (b) respectively. The position of the peaks for each film thickness and incident angle are shown in Table I.

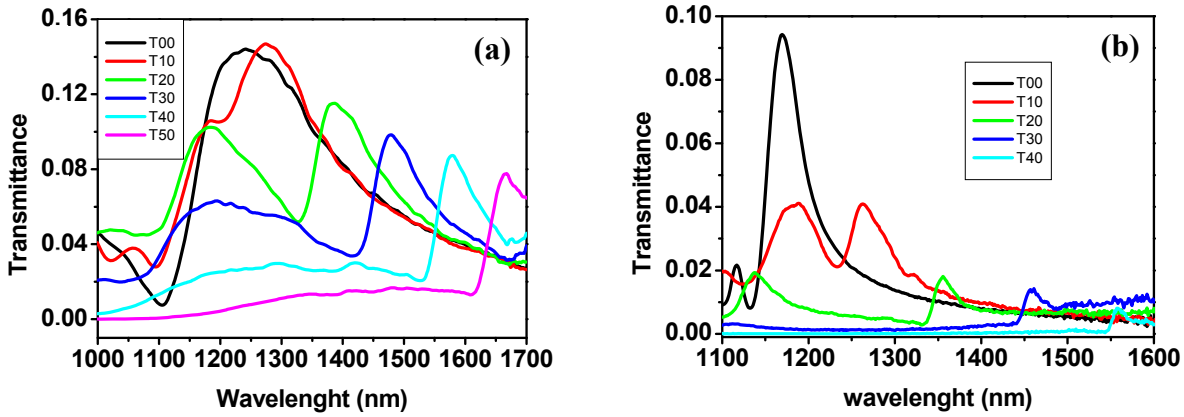

Fig. 8.Optical transmission spectra of the square array of holes (with 700 nm of period) as a function of the incident angle of the light. (a) Sample with Au film thickness of 100nm and (b) Sample with Au film thickness of 200nm.

Table. I. Wavelenghts of the plasmonic peaks for different incidence angles, film thickness, array periods and surrounding media, obtained from the Transmission spectra of Figure 7, 8 and 9.

Periodicity	thickness	Θ (°)	Peak: λ_{air}	Peak: $\lambda_{METHANOL}$	Δλ	Δλ/RIU
600 nm	100nm	0	1097 nm			
600 nm	200nm	0	997 nm			
700 nm	100nm	0	1241.1 nm	1375.1 nm	134 nm	347.15 nm
700 nm	200nm	0	1169.6 nm	1197.8 nm	28.2 nm	73.06 nm
700 nm	100nm	10	1273.6 nm	1502.5 nm	228.9 nm	593 nm
700 nm	200nm	10	1263 nm	1265.5 nm	2.5 nm	6.48 nm
700 nm	100nm	20	1386.7 nm	>1700 nm	>313.3 nm	>811.66 nm
700 nm	200nm	20	1355.5 nm	1400 nm	44.5 nm	115.3 nm
700 nm	100nm	30	1458.7 nm	1514.12 nm	55.42 nm	168.65 nm
700 nm	200nm	30	1458.8 nm	1513.3 nm	54.5nm	141.19 nm
700 nm	100nm	40	1579 nm			
700 nm	200nm	40	1558 nm			
700 nm	100nm	50	1667.5 nm			

In order to check the feasibility of the samples as sensors, we measure the zero-order transmission spectra through the squared array of holes (Λ=700nm and t=200nm) for the sample immersed in methanol (n=1.3286) and changing the incident angle of the light from 0 to 40^0. The results are shown in Figure 9. The values of the peaks exhibited in Figure 9 are shown in Table I. As it can be observed, from Table I, there is a shift in the plasmon resonance peak for the same sample (Λ=700nm and t=200nm) when the sample is immersed in methanol. This shift occurs because the resonance frequency depends on the dielectric constant of the both metal and surrounding dielectric[2].

The refractive index unit (RIU) factor measures the sensitivity of the plasmon resonance with the surrounding medium[6]. The corresponding RIU are shown also in Table I, for the samples with the same array period and different thickness. It can be observed that when we change the dielectric medium (from air to methanol), the 100-nm thick Au sample present

a RIU greater than the 200-nm thick Au sample, for all the incident angles. This occurs probably because the effective dielectric constant should depend on the metal film thickness.

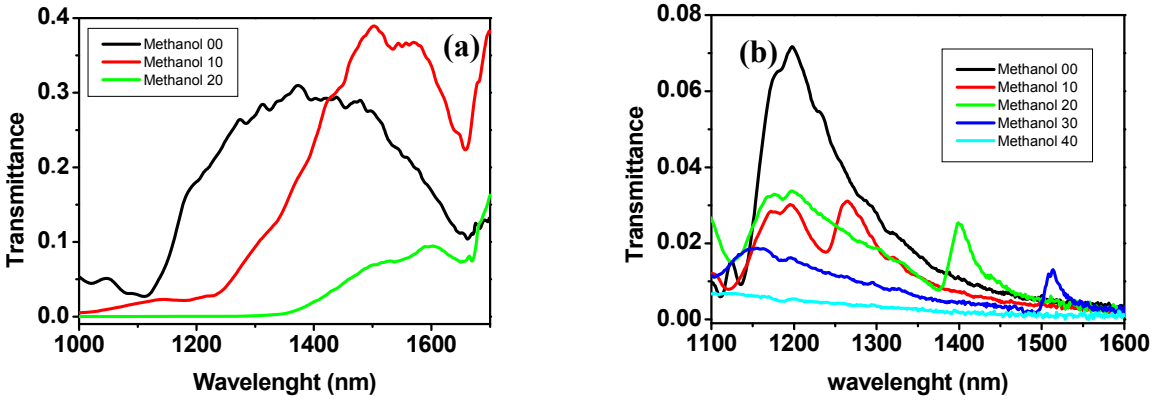

Fig. 9.Optical transmission spectra of the square array of holes in Methanol as a function of the incident angle of the light. (a) Sample with thickness of 100nm and (b) Sample with thickness of 200nm.

4- CONCLUSIONS

We demonstrate the fabrication of large areas plasmonic structures; appropriated for sensor applications, by combining holographic lithography and the evaporation of Au film. The samples were fabricated with different periods and thicknesses. The thickness of the Au film can be varied by controlling the time of the thermal evaporation. We observed that the thicker samples presented narrower plasmonic peaks, in the transmission spectra. The sensitivity to refractive index changes of the surrounding media, however, is poorer than that exhibited by thinner samples. Thus, thinner films are more appropriated for sensor applications. On the other hand, the periodicity of the lattice can be easily varied by changing the interference fringe period. This allows tailoring the peak of the plasmonic structure in a previously determined region of the spectrum in order to meet the desired application.

ACKNOWLEDGEMENTS

We acknowledge the financial support from the Fundação de Amparo a Pesquisa do Estado de São Paulo (FAPESP), Conselho Nacional de Pesquisa e desenvolvimento científico e tecnológico (CNPq) and FOTONICOM.

REFERENCES

[1] Ebbesen, T. W., Lezec, H. J., Ghaemy, H. F., Thio, T. and Wolff, P. A., "Extraordinary optical transmission through sub-wavelenght hole arrays," *Nature* 391, 667-669 (1998).

[2] Ghaemy, H. F., Thio, T., Grupp, D. E., Ebbesen, T. W., Lezec, H. J., "Surface plasmons enhance optical transmission through subwavelenght holes," *Phys. Rev. B*. 58, 6779-6782 (1998).

[3] Lal, S., Link, S. and Halas, N. J., "Nano-optics from sensing to waveguiding," *Nature Photonics* 1, 641-648 (2007).

[4] Barnes, W. L., Dereux, A. and Ebbesen, T. W., "Surface plasmon subwavelength optics," *Nature* 424, 824-830 (2003).

[5] Brolo, A. G., Arctander, E., Gordon, R., Leathem, B. and Kavanagh, K. L., "Nanohole-Enhanced Raman Scattering," *Nano Lett.* 4, 2015-2018 (2004).

[6] Brolo, A. G., Gordon, R., Leathem, B. and Kavanagh, K. L., "Surface plasmon sensor based on the enhanced light transmission through arrays of nanoholes in gold films," *Langmuir* 20, 4813-4815 (2004).
[7] Brueck, S. R. J., "Optical and Interferometric Lithography-Nanotechnology Enablers," Proc. IEEE 93, 1704-1721 (2005).
[8] Lai, N. D., Liang, W. P., Lin, J. H., Hsu, C. C. and Lin, C. H, "Fabrication of two- and three-dimensional periodic structures by multi-exposure of two-beam interference technique," *Opt. Express* 13, 9605-9611 (2005).
[9] Frejlich, J., Cescato, L., Mendes, G. F., "Analysis of an active stabilization system for holographic setup," Appl. Opt. 27, 1967-1976 (1988).